INT. J. NUM. METH. HEAT FLUID FLOW, VOL. 5, 33–48 (1995)

CONVECTIVE DISCRETIZATION SCHEMES FOR THE TURBULENCE TRANSPORT EQUATIONS IN FLOW PREDICTIONS THROUGH SHARP U-BENDS

T. BO, H. IACOVIDES AND B. E. LAUNDER

Mechanical Engineering Department, UMIST, Manchester, UK

ABSTRACT

This paper presents finite volume computations of turbulent flow through a square cross-sectioned U-bend of curvature strong enough ($Rc/D = 0.65$) to cause separation. A zonal turbulence modelling approach is adopted, in which the high-Re k–ε model is used over most of the flow domain with the low-Re, 1-equation model of k-transport employed within the near-wall regions. Computations with grids of different sizes and also with different discretization schemes, demonstrate that for this flow the solution of the k and ε equations is more sensitive to the scheme employed in their convective discretization than the solution of the mean flow equations. To avoid the use of extremely fine 3-Dimensional grids, bounded high order schemes need to be used in the discretization of the turbulence transport equations. The predictions, while encouraging, displayed some deficiencies in the downstream region due to deficiencies in the turbulence model. Evidently, further refinements in the turbulence model are necessary. Initial computations of flow and heat transfer through a rotating U-bend, indicate that at rotational numbers ($Ro = \Omega D/W_b$) relevant to blade cooling passages, the Coriolis force can substantially modify the hydrodynamic and thermal behaviour.

KEY WORDS Finite volume Turbulence Zonal modelling Convection

INTRODUCTION

This study is mainly concerned with numerical discretization issues that arise in finite volume computations of turbulent flow and convective heat transfer through U-bends of curvature strong enough to cause flow separation. Such flow passages are similar to the internal cooling passages of gas-turbine blades, where the flow and heat transfer are strongly influenced by the presence of sharp U-bends as well as by the orthogonal rotation of the blade. The overall objective of the research was to address turbulence modelling issues related to the computation of separated flows in strongly curved ducts without and with rotation. Turbulence modelling issues can, however, only be addressed when flow computations are free of significant numerical errors. The main aim of the present work was thus to produce numrically clean solutions of such flows in order to assess the adequacy of turbulence models currently employed in the computation of blade-cooling flows.

Turbulent flow through U-bends of square cross-section has been the subject of a number of numerical investigations. Most of the previous numerical studies have, however, been concerned with U-bends of milder curvature in which there is no flow separation. In some of the first studies that presented detailed comparisons between numerical computations and experimental data, Chang *et al.*[1] and Johnson[2] examined flow through a 180° bend of radius of curvature to

0961–5539/95/010033–16$2.00

Received November 1993
Revised April 1994

diameter ratio of 3.375, using the k–ε model to account for the effects of turbulence on the flow development. These studies relied on the use of semi-empirical wall laws (wall functions) to bridge the viscous sublayer and the buffer regions adjacent to the walls.

As a result of the curvature-induced secondary motion, a complex three-dimensional flowfield develops within a U-duct. These complex flow features were not fully captured by these early computations. In subsequent studies, Choi *et al.*[3] and Iacovides *et al.*[4] discarded the use of wall functions and integrated the mean flow equations across the wall sub-layer. A fine near-wall mesh was used in their place and the turbulent viscosity within the near-wall sublayer was obtained from Van-Driest's[5] version of the mixing length model. The near-wall mixing length model was matched to either a k–ε model of a second-moment algebraic stress model (*ASM*) outside the thin sublayer regions. This zonal modelling approach proved more successful in reproducing the complex flow structures present within curved ducts, especially when used with a second-moment closure in the main flow region. In a recent study, Breuer and Rodi[6] attempted to compute the same U-bend flow using Large Eddy Simulation. The resulting comparisons indicate that this approach is not at present suitable for the prediction of such flows.

For U-bends of stronger curvature, Besserman and Tantikut[7] presented comparisons between computed and measured heat transfer coefficients for a square cross-sectioned 180° bend of a radius of curvature to diameter ratio of 1.59. The predictions were obtained using a k–ε turbulence model. Across the near-wall regions two alternatives were tested; the wall function approximation and also, as in References 3 and 4, a zonal modelling approach with the Van-Driest mixing length model used to account for the effects of sublayer turbulence. Again, the zonal model returned more realistic predictions than the model relying on the wall function approximation. Heat transfer predictions along the inner and outer walls were, however, in need of further improvement. Flow and heat transfer through a U-bend of tighter curvature, similar to that of the present study, have also been recently computed by Xia and Taylor[8]. A finite element solution procedure was employed with a one-equation effective-viscosity model of turbulence transport. Comparisons with some of the available mean flow and heat transfer data indicated that some of the measured flow features were reproduced by these computations. In accord with earlier views, Xia and Taylor concluded from their study that the use of wall functions was inappropriate.

In the present study the authors main objective has been to assess the effectiveness of a zonal two-equation (k–ε) model for computations of flows through tight U-bends. A common practice in turbulent flow computations using finite-volume methodology, has been to use higher order schemes, such as *QUICK*[9], for the discretization of the mean flow equations while retaining a low order upwind scheme, like *HYBRID*[10], for the convective discretization of turbulence variables such as k and ε. This strategy arose from the belief that, because the k and ε equations were dominated by large source terms, the convective transport of these variables and its discretization were of secondary importance. It is certainly the case that, on occasions, the discretization of the turbulence equations has been found to have only a minor effect on the computed flow field[11]. However, in separated flows it seemed at least possible that the strong imbalance between the positive and negative source terms in the turbulence transport equations would lead to circumstances in which the local values of k and ε were highly dependent on convective transport. In that event, one would expect that the usual upwind differencing of k and ε would lead to serious errors in prediction.

The above question is one of the principal issues examined in the present paper. As remarked earlier, the flow chosen is that of the internal blade-cooling passage which, because of its separated flow regions, is a most challenging flow to compute. Indeed, because of the flow's 3-Dimensionality, one needs to achieve high discretization accuracy to achieve accurate solutions with an acceptable number of grid nodes. Whether or not that high accuracy is demanded in the turbulent transport equations as well as in the mean flow variables is one of the issues examined in this paper. Our choice of a high-order non-diffusive discretization scheme is *LODA*[12] which amounts to employing the well known *QUICK* scheme except adjacent to extrema, thereby avoiding the problem of under- or overshoots to which the *QUICK* scheme is susceptible.

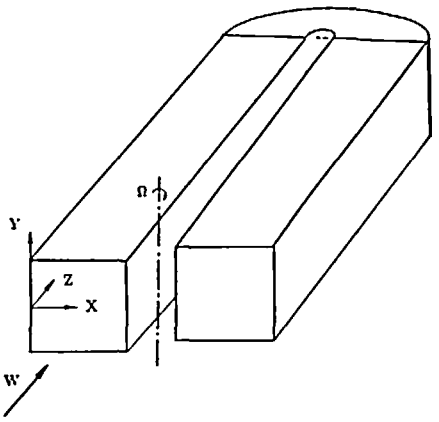

Figure 1 Flow geometry

In the present study, these numerical issues are addressed using a relatively simple effective viscosity model of turbulence transport. This we felt was an appropriate starting point and any conclusions reached could reasonably be extended to more refined models. Moreover, since effective viscosity models are still those most widely used by industry, it is important to establish how reliable their predictions are in the case of blade-cooling flows.

Even though detailed flow measurements were only available for a stationary U-bend, computations are also presented for a rotating U-bend cases, as shown in *Figure 1*, in order to demonstrate how important Coriolis effects are likely to be in real cooling passage flows.

FLOW EQUATIONS

All equations are expressed here in Cartesian tensor notation, for a rotating frame of reference. In the actual computations the Cartesian version of these equations was only employed within the upstream and downstream tangents. Within the U-bend the cylindrical polar version of the flow equations was used.

Mean motion

Continuity

$$\frac{\partial}{\partial x_i}(\rho U_i) = 0 \tag{1}$$

Momentum Transport

$$\frac{\partial}{\partial x_i}(\rho U_i U_j) = -\frac{\partial P}{\partial x_i} + \frac{\partial}{\partial x_j}\left[(\mu + \mu_t)\left(\frac{\partial U_i}{\partial x_j} + \frac{\partial U_j}{\partial x_i}\right)\right] - 2\rho\varepsilon_{ijp}\Omega_p U_j - \rho[\Omega_j X_j \Omega_i - \Omega_j X_i \Omega_j] \tag{2}$$

Enthalpy Transport

$$\frac{\partial}{\partial x_j}(\rho U_j \Theta) = \frac{\partial}{\partial x_j}\left[\left(\frac{\mu}{\sigma} + \frac{\mu_t}{\sigma_\Theta}\right)\frac{\partial \Theta}{\partial x_j}\right] \tag{3}$$

where μ_t is the turbulent viscosity, σ is the molecular Prandtl number and σ_Θ the turbulent

Prandtl number. The quantity Ω denotes the rotation vector and X the distance from the axis of rotation.

Turbulent flow equations

As indicated previously, an effective viscosity model (*EVM*) of turbulence transport has been employed because of its simplicity in relation to the more advanced second-moment closures. It is thus easier to address discretization issues related to the prediction of U-bend flows. As in our earlier computations of curved duct flows[3,4], in order to resolve the strong secondary motion of the near-wall regions, the near-wall turbulence is modelled through the use of low-Reynolds number turbulence models. In this first attempt to compute these flows, the k–ε model was adopted in the core region of the duct and this was matched to a low-*Re* 1-equation (k-transport) model close to the wall.

The specific modelled forms are as follows:

(a) High-Re k–ε

k-*Transport equation*

$$\frac{\partial}{\partial x_j}(\rho U_j k) = \frac{\partial}{\partial x_j}\left[\left(\mu + \frac{\mu_t}{\sigma_k}\right)\frac{\partial k}{\partial x_j}\right] + P_k - \rho\varepsilon \tag{4}$$

where:

$$P_k = \mu_t \frac{\partial U_i}{\partial x_j}\left(\frac{\partial U_i}{\partial x_j} + \frac{\partial U_j}{\partial x_i}\right); \qquad \mu_t = c_\mu \rho k^2/\varepsilon \tag{5}$$

ε-*Transport equation*

$$\frac{\partial}{\partial x_j}(\rho U_j \varepsilon) = \frac{\partial}{\partial x_j}\left[\left(\mu + \frac{\mu_t}{\sigma_\varepsilon}\right)\frac{\partial \varepsilon}{\partial x_j}\right] + c_{\varepsilon 1}\frac{\varepsilon}{k}P_k - \rho c_{\varepsilon 22}\frac{\varepsilon^2}{k} \tag{6}$$

(b) Near-wall 1-equation model, (Wolfshtein[13])

Within the near-wall regions, equations (4) and (5) are retained but the dissipation rate, ε, and the effective viscosity, μ_t, are obtained from prescribed length scales according to:

$$\varepsilon = k^{\frac{3}{2}}/l_\varepsilon \qquad \mu_t = \rho c_\mu \sqrt{k} l_\mu \tag{7}$$

The length scales l_ε and l_μ are obtained from the near-wall distance Y according to:

$$l_\varepsilon = 2.55Y(1 - \exp(-0.263y^*) \tag{8}$$

$$l_\mu = 2.55Y(1 - \exp(1 - 0.061y^*) \tag{9}$$

where $y^* = Yk^{1/2}/\nu$ is the dimensionless wall distance.

The constants that appear in the above equations have the values shown in *Table 1* while in all cases the molecular Prandtl number has been taken as 0.70.

NUMERICAL ASPECTS

Computations have been carried out using a 3-Dimensional finite volume code. It uses the pressure-correction procedure (*SIMPLE*) and employs a staggered grid arrangement. Full details

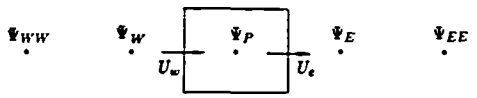

Figure 2 One-dimensional stencil

can be found in Bo[4]. As already mentioned, the discretization of convective transport has received particular attention. Within the control volume approach, the problem of convective discretization amounts to that of finding the value of the discretized variable, Ψ, at the control volume faces, as indicated in *Figure 2*. In the *HYBRID* scheme, when the cell-face Peclet number is less than 2 a central-difference interpolation is used, but for the higher values the upwind scheme is employed. In the *QUICK* scheme, a quadratic inter-nodal variation is used. Three nodal values are thus needed to fix the assumed parabolic variation, two of which are placed on the upwind side and one on the downstream site. In order to prevent numerical oscillations, especially in the solution of the k and ε transport equations, the *QUICK* scheme needs to be bounded. In this study the relatively simple *LODA*[12] bounding procedure is employed. For cells in which the discretized variable has a local maximum or minimum value along any direction, the interpolated cell face values along the relevant direction are obtained by blending the interpolated values of the *QUICK* scheme with those resulting from use of the upwind scheme. For the control volume of *Figure 2*, if:

$$\hat{\Psi}_p = (\Psi_p - \Psi_W)/(\Psi_E - \Psi_W) \tag{10}$$

then:

For $\hat{\Psi}_p > 1$ or $\hat{\Psi}_p < 0$

$$\Psi_e = \gamma_e \Psi_e^Q + (1 - \gamma_e)\Psi_e^U; \qquad \Psi_w = \gamma_w \Psi_w^Q + (1 - \gamma_w)\Psi_w^U \tag{11}$$

The subscripts Q and U refer to the *QUICK* and upwind interpolation values respectively. The blending factor value, γ, is obtained from the Peclet number (*Pe*) at the relevant cell face:

$$\gamma e = \min [1, Pe_e^{-1}] \tag{12}$$

To ensure consistency of coefficients, at each face, the minimum γ value indicated by the two adjacent cells is adopted.

To improve numerical stability, Zhou and Leschziner[12] under-relaxed the blending factor values. In this study, in order to save storage, only the blending factor values for streamwise convection are under-relaxed. Furthermore under-relaxation is performed only at locations where the current iteration γ values are higher than those of the previous iteration. For the k and ε equations a further stabilization step was developed during the course of this investigation to prevent negative values for k and ε in the *LODA* solutions. A maximum cell blending factor value, γ_{max}, is prescribed for each control volume. This maximum γ value, at each control volume, is obtained by requiring that a point-by-point solution of the discretized equations for k and ε yields positive values. If the upwind and *QUICK* discretized equations are expressed as:

$$A_p^U \Psi_p = \sum A_{nb}^U \Psi_{nb} + S_\Psi \qquad A_p^Q \Psi_p = \sum A_{nb}^Q \Psi_{nb} + S_\Psi^Q + S_\Psi \tag{13}$$

by blending the two schemes:

$$[(1 - \gamma)A_p^U + \gamma A_p^Q]\Psi_p = \sum [(1 - \gamma)A_{nb}^U + \gamma A_{nb}^Q]\Psi_{nb} + \gamma S_\Psi^Q + S_\Psi \tag{14}$$

The maximum value of γ, γ_{max}, is then determined by requiring $\Psi_p \geqslant 0$. If the *LODA* criteria, equation (12), return γ values at the cell faces that are higher than the control volume γ_{max}, then these cell face values of γ are reduced to γ_{max}.

COMPUTATIONAL DETAILS

The case examined is that of a hydrodynamically and thermally fully developed flow entering a heated U-bend of square cross-section and of curvature ratio $R_c/D = 0.65$. The flow Reynolds number is 100,000. A uniform heat flux is applied at the duct walls. The computational domain in this study begins three duct diameters upstream of the bend and extends 8 diameters downstream of it. The flow is assumed to be symmetric about the geometric plane of symmetry and thus only one half of the duct cross-section needs to be considered, both for the stationary and also for the rotating case computed in this study.

Four grid arrangements have been employed; a coarse grid consisting of a 35 × 67 × 103 nodes, in the normal, radial and streamwise directions respectively, two medium size grids each employing 35 × 67 × 133 and a fine grid of 35 × 77 × 177 nodes. Earlier U-bend studies using similar turbulence models[5] have shown that the 35 × 67 grid distribution, shown in *Figure 3(c)*, is able to keep numerical errors to sufficiently low levels. In the coarse grid as shown in *Figure 3(b)*, 13 planes were located within the upstream section, 40 planes within the U-bend and the remaining 50 planes were located in the downstream section. In the first of the 2 medium grids, all the extra 30 planes were placed in the downstream section. In the second medium sized mesh, most of the extra 30 planes were located within the U-bend resulting in a streamwise grid distribution in which there were 19 planes in the upstream section, 60 planes in the U-bend and 54 planes in the downstream section. Finally, for the fine grid, the 10 extra radial nodes were placed in the outer half of the duct cross-section and the streamwise grid distribution consisted of 23 planes in the upstream section, 100 planes within the bend and 54 planes downstream. For the medium sized mesh 40 *Mb* of *CPU* memory were required during the execution of the computations and 24.5 seconds of *CPU* time were needed on an *AMDAHL VP1100* mainframe per iteration over the domain.

For each grid three computations have been performed: one in which the *HYBRID* discretization scheme was used for all the transport equations; one in which *LODA* was used for

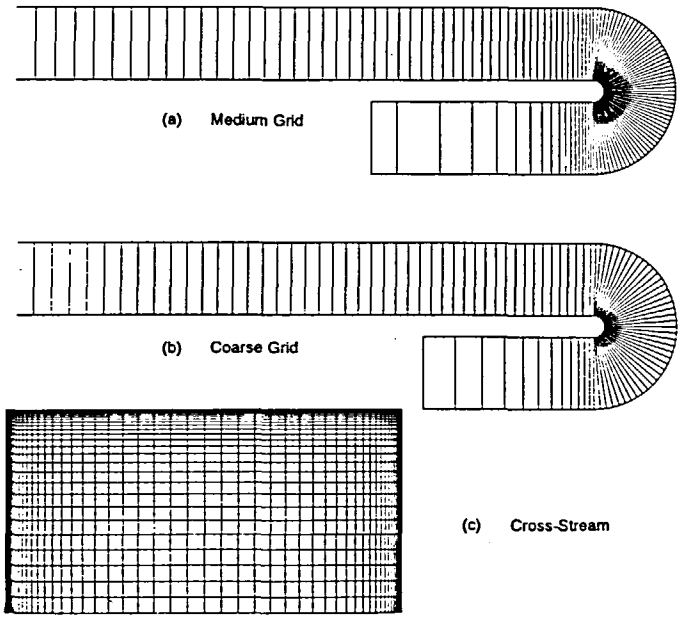

Figure 3 Grid distributions

Table 1 Turbulence model constants

$c_{\varepsilon 1}$	$c_{\varepsilon 2}$	c_μ	σ_k	σ_ε	σ_θ
1.44	1.92	0.09	1	1.22	0.9

Table 2 List of computations performed

Grid size	Coarse 35 × 67 × 103	Medium 1 35 × 67 × 133	Medium 2 35 × 67 × 133	Fine 35 × 77 × 177
Discretization schemes	1 *HYBRID* on all variables	1 *HYBRID* on all variables	1 *HYBRID* on all variables	1 *HYBRID* on all variables
	2 *LODA* on mean flow variables and *HYBRID* for k and ε	2 *LODA* on mean flow variables and *HYBRID* for k and ε	2 *LODA* on mean flow variables and *HYBRID* for k and ε	
	3 *LODA* on all variables	3 *LODA* on all variables	3 *LODA* on all variables	

the mean flow equations while *HYBRID* was retained for k and ε; and one in which *LODA* was employed for all flow variables.

The different grids tested and the discretization schemes employed wuth each grid are summarized in *Table 2.*

RESULTS AND DISCUSSION

The overall mean flow development is first presented in the predicted vector plots of *Figures 4* and *5*. The vector plots of *Figure 4* present the streamwise flow development along the symmetry plane (*4(a)*) and at a plane half-way between the symmetry plane and the top wall (*4(b)*). The effects of the strong streamwise pressure gradients, at the bend entry and exit appear to dominate

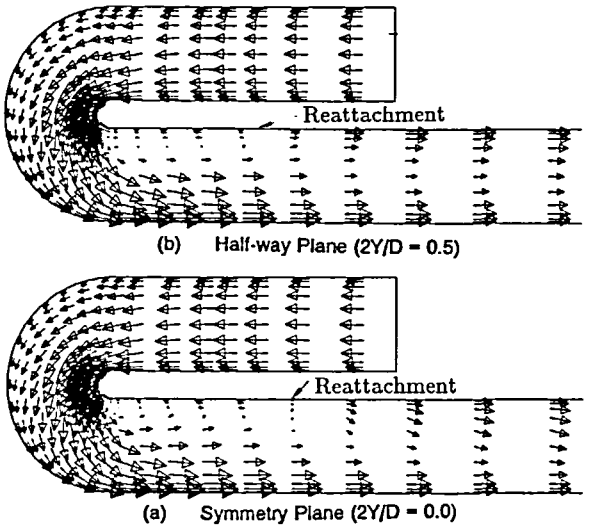

Figure 4 Predicted streamwise vector plots using *LODA* (a) Symmetry plane ($2Y/D = 0.0$) (b) Half-way plane ($2Y/D = 0.5$)

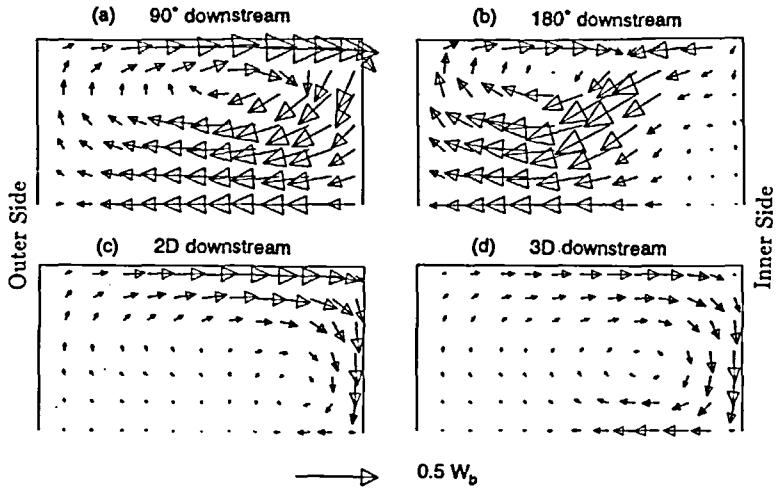

Figure 5 Predicted cross-duct vector plots using *LODA*

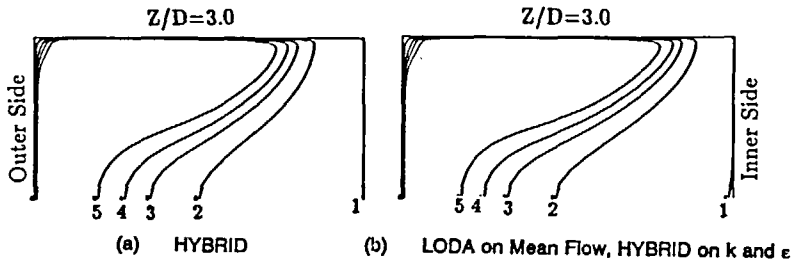

Figure 6 Coarse grid predictions of streamwise flow field at 3 diameters downstream of the bend

the flow development. A separation bubble is formed downstream of the bend along the inner wall. Along the symmetry plane, the separation region extends to about 2 hydraulic diameters downstream of the bend while, at the half-way plane, it is somewhat shorter. As shown in *Figure 5*, the secondary motion that prevails over the first three downstream diameters, transfers high momentum fluid along the top wall, from the outer to the inner side of the downstream section. This accounts for the shorter recirculation length along the 'half-way plane' (*Figure 4b*) and the rapid acceleration predicted along the inner wall after reattachment.

Figure 6 shows two sets of predicted streamwise velocity contours, at 3 hydraulic diameters downstream of the bend, computed with the coarse mesh; one set was obtained using *HYBRID* and the other set by using *LODA* on the mean flow equations while retaining *HYBRID* for k and ε. These two sets of computations appear to give very similar results. This comparison, typical of more detailed comparisons not presented here, suggests that even the coarsest grid used in this study, is fine enough to keep convective discretization errors in the numerical solution of the *mean flow* equations to unimportant levels.

Grid refinement downstream of the U-bend led to computed flow fields, not shown here, identical to those of the coarse mesh, *Figure 3b*, for all the different discretization practices. The streamwise grid density downstream of the bend is therefore found to be adequate for the discretization of all equations. The symmetry plane profiles of *Figure 7* on the other hand, reveal

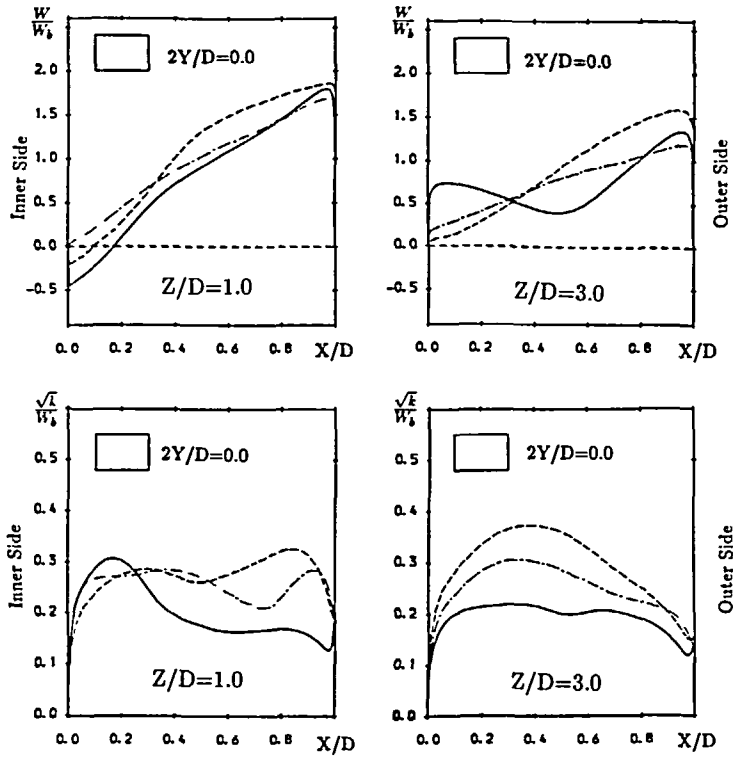

Figure 7 Symmetry plane profiles at 1 and 3 diameters downstream. —— 2nd medium grid with *LODA* in all equations; ---- 2nd medium grid *HYBRID*; -·- fine grid *HYBRID*

that the streamwise grid density within the bend and also the convective discretization of k and ε, do affect the resulting computations. The *HYBRID* solution of the second 'medium mesh' is different from the corresponding coarse grid prediction of *Figure 6*. As the find grid predictions indicate, none of the *HYBRID* solutions can be regarded as grid independent. The medium grid solution with the *LODA* scheme employed on all the transport equations, suggests that the convective discretization of the turbulence transport equations is especially important. Even, as suggested by *Figure 6*, when the grid appears to be fine enough for a low order discretization scheme to be safely used for the mean flow equations, discretization errors can still arise from the solution of the k and ε equations. Due to the coupling between the equations for k, ε and the mean velocities, errors generated in the solution of the k and ε transport equations subsequently contaminate the mean flow solution as well. The computations of the two medium sized grids suggest that the errors in the k and ε solutions appear to be generated within the bend, where strong source (generation and dissipation) terms create steep streamwise gradients in the k and ε distributions and where there is also a strong cross-duct motion. The errors are then convected downstream of the bend where, due to flow separation and the absence of any strong mean flow influences like curvature force, the mean flow development is mainly controlled by the turbulence field.

In *Figure 8*, cross-stream profiles for the streamwise velocity and of the turbulence intensity of the *LODA* solutions for the coarse and medium grids, are presented at 1 and also at 3 diameters downstream of the bend. These comparisons reveal that when the higher order discretization scheme is applied to all transport equations, the U-bend predictions are no longer significantly affected by grid refinement. It is thus demonstrated that in the prediction of turbulent

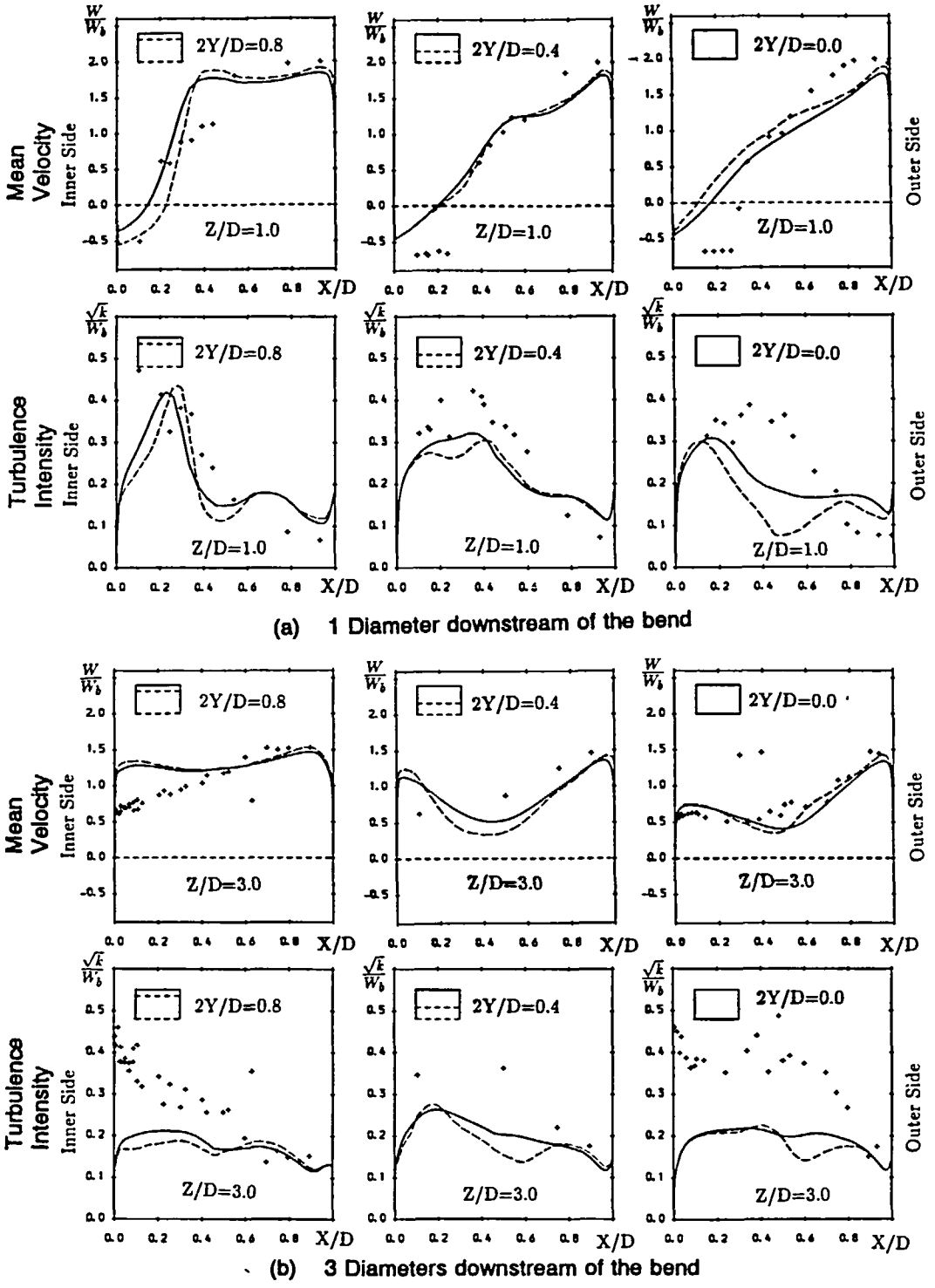

Figure 8 Comparisons between *LODA* predictions and measurements. —— 2nd medium grid *LODA*; ---- coarse grid *LODA*; + + ·· data [15]

flow through tight U-bends it is necessary to employ high order schemes for the discretization of *all* the transport equations if the use of extremely fine 3-Dimensional grids is to be avoided.

An impression of the suitability of the k–ε/1-equation model may be gained by comparing computational results with *LODA* data[15], shown in *Figure 8*, and also through subsequent heat-transfer comparisons. At 1-diameter downstream of the bend, the streamwise velocity field is fairly well predicted, though the size of the separation bubble is somewhat under-estimated. This turbulence model also returns a reasonble turbulence intensity distribution, showing high turbulence levels on the inner side of the duct where the flow direction is reversed. The predicted turbulence levels near the outer wall are however higher than the measured ones. These predictive failures are believed to be due to the inability of the 1-equation model to account for variations in the turbulent length scale brought about by transport effects. Near-wall turbulence transport becomes important in regions of flow separation and also in regions of severe streamwise flow acceleration. Both these phenomena are present at the bend exit. Nevertheless at 1.0 diameter downstream of the bend, the hydrodynamic predictions are surprisingly close to the data. At 3.0 diameters downstream of the bend (by which point the flow has reattached) there are greater discrepancies between the computations and the measurements. Near the upper wall there is too little variation of velocity between the inside and outside. The computed turbulence levels are considerably lower than the measured ones due to the under prediction of the turbulence levels at the edge of the separation bubble, *Figure 8a*.

Turning attention to heat-transfer comparisons, the measured[16] and predicted distributions of the local heat-transfer coefficient along the top wall are shown in *Figure 9*. The model

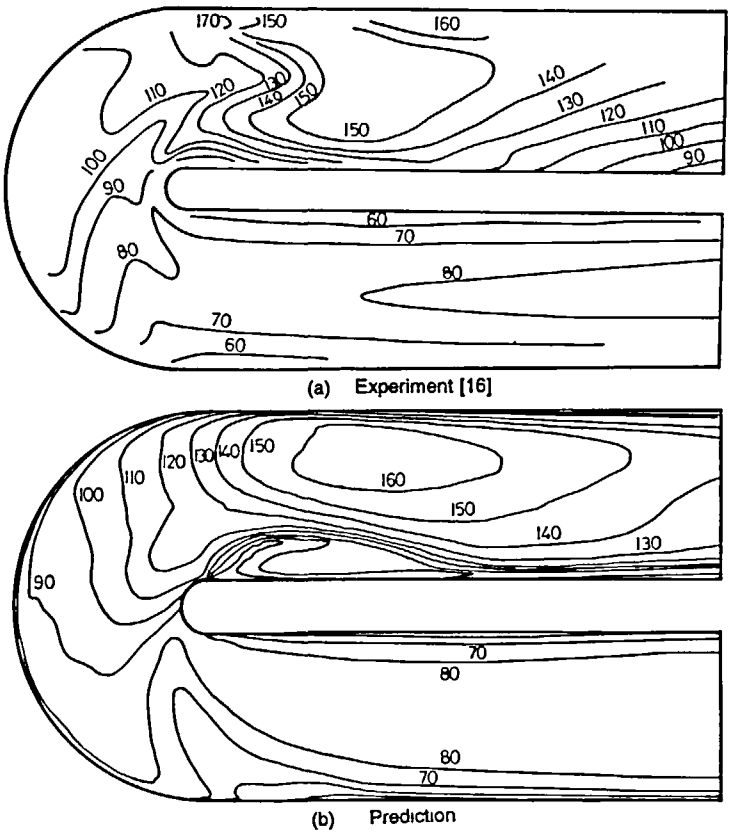

Figure 9 Distribution of the local wall heat flux coefficient along the top wall

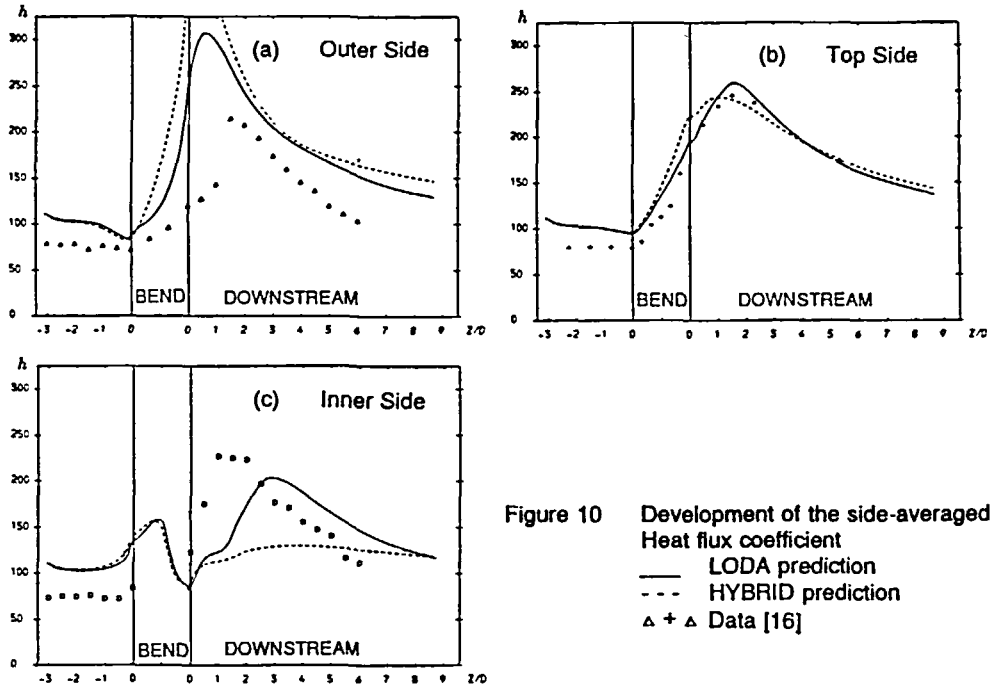

Figure 10 Development of the side-averaged Heat flux coefficient
—— LODA prediction
- - - HYBRID prediction
△ + △ Data [16]

Figure 10 Development of the side-averaged heat flux coefficient. —— *LODA* prediction; --- *HYBRID* prediction; △ + △ data [16]

reproduces the measured thermal behaviour reasonably well. The levels, and the shapes of the predicted contours are close to those of the measurements. The main discrepancy appears to be near the inner side, downstream of the bend exit, where the prediction fails to return the high heat transfer levels present in the vicinity of the separation region.

For the other walls comparisons for the side-averaged heat flux values are performed. *Figure 10* shows that significant and systematic differences between measurement and prediction occur along the curved inner and outer walls and downstream therefrom. First, a comparison between the *HYBRID* and *LODA* heat-transfer predictions with a medium grid highlights how sensitive the thermal solution is to the discretization of the k and ε equations. The computed heat flux coefficients are based on the difference between the local wall and the local fluid bulk temperatures while, in the measured values, a set of point gas temperature measurements was used to replace the local bulk temperature over different sections of the duct. This difference in definitions accounts for the discrepancies between computations and measurements upstream of the bend. As observed in *Figure 9*, the model provides a very realistic estimate of the average heat flux coefficient along the top wall. The outer wall heat-transfer rate is, on the other hand, significantly over-predicted in the vicinity of the bend exit while, along the inner side, downstream of the bend, the predicted heat transfer levels do not rise as rapidly or as highly as the measured values. These inabilities of the turbulence model to compute the correct heat transfer levels in the downstream region, are consistent with the failure of the near-wall model to return the correct turbulence levels over the same region. These comparisons are consistent with those of Besserman and Tanrikut[6] in which the k–ε/mixing length model was used and the U-bend was of a somewhat milder curvature. Earlier studies carried out within the authors' group, concerning curved ducts of milder curvature (References 3, 17 and 18), demonstrate that the inclusion of second-moment closures can significantly improve the prediction of flow and heat transfer in three-dimensional curved

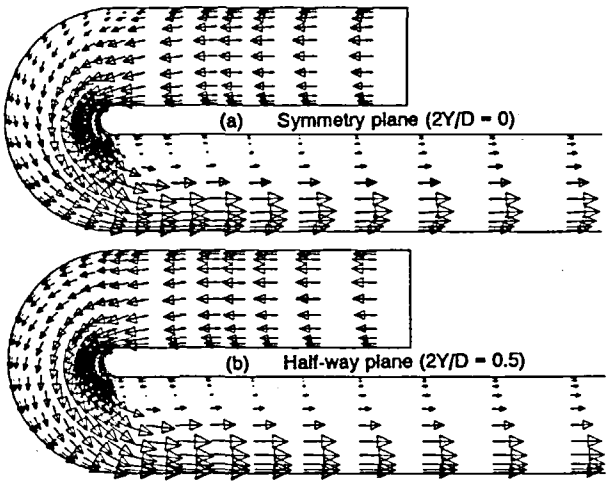

Figure 11 Predicted streamwise vector plots for positive rotation at $Ro = 0.12$

passages. Moreover, earlier work on two-dimensional flows (References 19 and 20), revealed that in order to reproduce the effects of either flow acceleration or flow separation on near-wall turbulence it becomes necessary to use near-wall models which involve transport equations for at least two turbulence quantities. These arguments suggest that the use of a two-equation low-Reynolds number model in the near-wall zone becomes necessary with, possibly, a second-moment closure in the main flow to try and account for the effects of the strong streamline curvature that is present in this flow.

Having demonstrated some of the limitations of the k–ε/1-equation model when it is used in the computation of flow and heat transfer in sharp U-bends, it was nevertheless felt that it would be informative to use this numerical procedure to explore the effects of orthogonal rotation on the hydrodynamic and thermal development of such flows. Further computations were therefore obtained, using the second of the 'medium grids' for fully-developed flow entering a U-bend that rotates positively at a Rotation number ($Ro = \Omega D/W_b$) of 0.12. For a positive rotation, shown in *Figure 1*, the Coriolis force acts in the same direction as the curvature force within the U-bend. The plane of symmetry is thus preserved and one would expect that the effects of curvature on the flow would be augmented.

Figure 11 shows the effects of positive rotation on the mean flow development. The differences in the velocity distribution (between the rotating and the stationary case of *Figure 4*) at the bend entry are mainly caused by the fact that entry conditions, at 3 hydraulic diameters upstream of the bend, are now different, corresponding to those of fully developed flow in a rotating duct. The Coriolis effects on the flow development are more prominent in the downstream region. Along the symmetry plane, the recirculation bubble is initially wider in the presence of positive rotation but its predicted length remains unchanged relative to that of the stationary U-bend. Downstream of reattachment the positive Coriolis force slows down the rate of recovery, maintaining the faster fluid along what was the outer side and the slower fluid along the inner side. The Coriolis force has similar effects on the downstream flow development along the half-way plane (*Figure 11b*), where the separation bubble is now longer compared with the stationary case (*Figure 4b*). It is also worth noting that, in the presence of rotation, the predicted mean flow development downstream of the U-bend was found to be less sensitive to the convective discretization of the turbulence transport equations. This finding is not surprising because, due to the presence of the Coriolis force, the influence of transported turbulence on the development of the downstream flow is now less important.

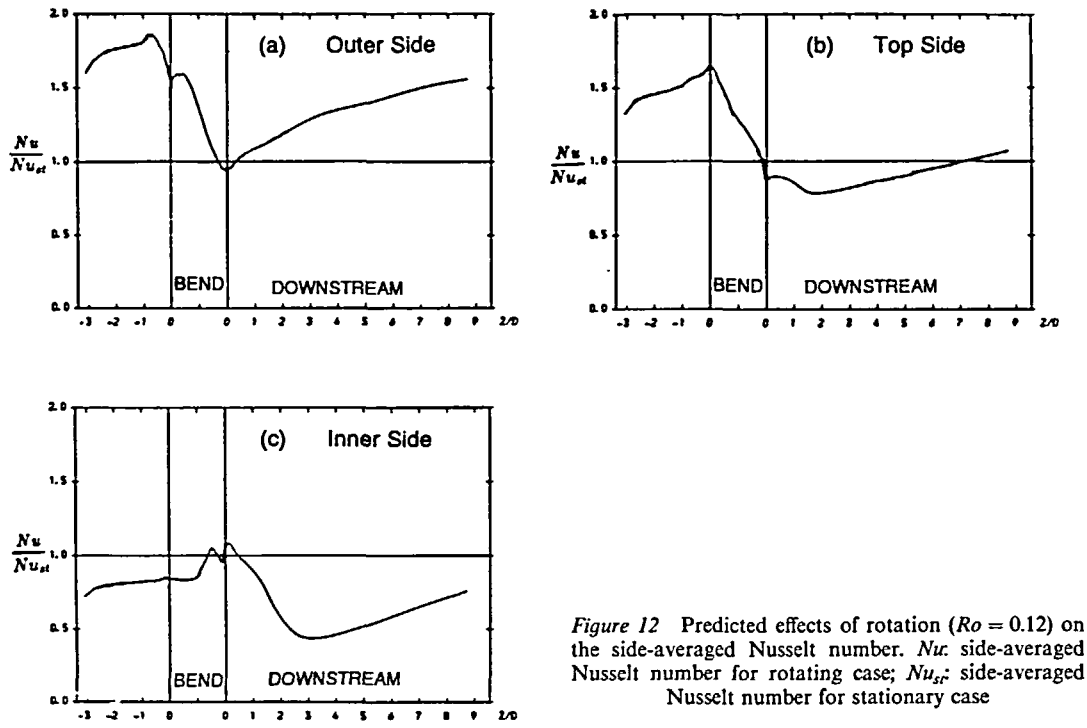

Figure 12 Predicted effects of rotation ($Ro = 0.12$) on the side-averaged Nusselt number. Nu: side-averaged Nusselt number for rotating case; Nu_{st}: side-averaged Nusselt number for stationary case

The effects of rotation on the predicted thermal behaviour are summarized in the plots of *Figure 12*, which present the development of the side-averaged Nusselt number normalized with the corresponding values of the stationary U-bend. In the upstream section, the normalized Nusselt number levels are initially those corresponding to fully developed flow in a straight duct rotating in orthogonal mode. As shown in earlier studies[21], orthogonal rotation in a straight duct increases heat-transfer rates along the sides that, for positive rotation, coincide with the bend top and outer sides and reduces heat transfer rates along the bend inner side. Within the U-bend the normalized Nusselt numbers on all sides tend towards unity, revealing that the effects of strong curvature overshadow those of rotation at $Ro = 0.12$. Downstream of the bend, the plots of *Figure 12* indicate that the recovery to the fully-developed heat-transfer levels is non-monotonic, particularly along the inner side. The present computations demonstrate clearly that, even in bends with very tight curvature orthogonal rotation at $Ro = 0.12$ causes significant changes to the flow and thermal development in U-bends. Moreover these comparisons indicate that effects (on flow and heat transfer) caused by the combined action of the Coriolis and curvature forces, cannot always be deduced by simply considering how curvature and rotation separately influence duct flow and heat transfer.

CONCLUSIONS

In the computation of flow through U-bends which are tight enough to cause flow separation, the convective discretization of the turbulence transport equations is shown to be of primary importance to the overall numerical accuracy of the solution. Bounded high order schemes for the discretization of the turbulence transport equations can significantly reduce the grid size necessary for an error free solution. Though this conclusion has been arrived at through a set of

computations involving the k–ε model, it is expected to apply to other turbulence models that are at a two-equation or a more advanced level.

The k–ε/1-equation model has produced numerical predictions that are, on the whole, in encouraging agreement with experiment. Significant predictive deficiencies have, however, been identified in the region of the bend exit. The combination of flow separation on the inner side and strong acceleration along the outer side of the bend exit requires, at the very least, a near-wall model that accounts for the transport of turbulent length scale within the near-wall region. Computations for a rotating U-bend indicate that, at rotational rates comparable to those encountered in blade-cooling passages, orthogonal rotation can significantly modify the flow and thermal development through the U-bend. As *Figure 12* has shown, however, the two effects combine in a highly non-linear way.

ACKNOWLEDGEMENTS

The research has been jointly supported by Rolls-Royce plc and RAE Pyestock under Research Brochure BID 2-125 D and is published by permission. Some of the finest grid computations were undertaken on Rolls-Royce's computers. We would like to thank Prof. Peter Stow for finding this practical solution to our difficulty of accessing adequate computer core and Mr. John Coupland for providing considerable practical assistance in executing these computations. The manuscript has been produced with appreciated care by Mr. Michael Newman.

REFERENCES

1 Chang, S. M., Humphrey, J. A. C., Johnson, R. W. and Launder, B. E. Turbulent momentum and heat transport in flow through a 180° bend of square cross-section, *Proc. 4th Symp on Turbulent Shear Flows*, pp. 620–625, Karlsruhe (1983)

2 Johnson, R. W. *Turbulent Convecting Flow in a Square Duct with a 180° Bend*, PhD Thesis, Faculty of Technology, University of Manchester (1984)

3 Choi, Y-D., Iacovides, H. and Launder, B. E. Numerical computation of turbulent flow in a square-sectioned 180° bend, *ASME J. Fl. Engrg.*, **111**, 59 (1989)

4 Iacovides, H., Launder, B. E., Loizou, P. A. and Zhao, H. H. Turbulent boundary-layer development around a square-sectioned U-bends: measurement and computation, *ASME J. Fl. Engrg.*, **112**, 409 (1990)

5 Van Driest, E. R. On turbulent flow near a wall, *J. Aero. Soc.*, **23**, 1007 (1956)

6 Besserman, D. L. and Tanrikut, S. Comparison of heat transfer measurements with computations for turbulent flow around a 180° bend, *ASME, 91-GT-2, Int. Gas-Turbine Aeroengine Congress and Exposition*, Orlando, Florida, 3–6 June (1991)

7 Breuer, M. A. and Rodi, W. Large-eddy simulation of turbulent flow through a straight square duct and a 180° bend, *The First ERCOFTAC Workshop on Direct and Large-Eddy Simulations*, V3, Session 5(a), University of Surrey (1994)

8 Xia, J. Y. and Taylor, C. The prediction of turbulent dlow and heat transfer in a tight square-sectioned 180° bend, *Proc of 8th Int. Conf. on Numerical Methods in Lam. and Turb. Flows*, Swansea (1993)

9 Leonard, B. P. A stable and accurate convective modelling procedure based on quadratic interpolation, *Comput. Meth. Appl. Mech. Engrg.*, **19**, 59–98 (1979)

10 Spalding, D. B. A novel finite-difference formulation for differential expressions involving both first and second derivatives, *Int. J. Num. Meth. Eng.*, **4**, 551 (1972)

11 Lien, F-S. *Computational Modelling of 3D Flow in Complex Ducts and Passages, PhD Thesis*, Faculty of Technology, University of Manchester (1992)

12 Zhou, H. and Leschziner, M. A. A local oscillation-damping algorithm for higher order convection schemes, *Comput. Meth. Appl. Mech. Engrg.*, **67**, 355 (1988)

13 Wolfshtein, M. The velocity and temperature distribution in one-dimensional flow with turbulence augmentation and pressure gradient, *Int. J. Heat and Mass Transfer*, **12**, 301 (1969)

14 Bo. T. *The Computation of Flow and Heat Transfer in Rotating Ducts and U-Bends, PhD Thesis*, Faculty of Technology, University of Manchester (1992)

15 Hicklin, D. J. Experimental velocity and turbulence measurements in a perspex 180° bend model using a Polytec lazer anemometer, Rolls-Royce internal report, GN 29335 (1988)

16 Davenport, R. Innovative use of thermochronic liquid crystals for turbine-blade cooling passage flow visualisation and heat transfer measurements, *European Propulsion Forum, Modern Techniques and Developments in Engine and Component Testing*, Bath, UK (1989)
17 Abou-Haidar, N. I., Iacovides, H. and Launder, B. E. Computational modelling of turbulent flow in S-bends, AGARD, Conf. Proc. 510, CFD Techniques on Propulsion Applications, San, Antonio, Texas (1991)
18 Iacovides, H. and Launder, B. E. The computation of convective heat transfer in a 180° pipe bend, *ICHMT. Int. Symp. on Heat Transfer in Turbomachinery*, Athens (1992)
19 Jones, W. P. and Launder, B. E. The prediction of laminarization with a two-equation model of turbulence, *Int. J. Heat & Mass Transfer*, **15**, 301 (1972)
20 Yap, C. R. *Turbulent Heat and Momentum Transfer in Recirculating and Impinging Flows, PhD Thesis*, Faculty of Technology, University of Manchester (1987)
21 Iacovides, H. and Launder, B. E. Parametric and numerical study of fully-developed flow and heat transfer in rotating rectangular ducts, *ASME J. Turbomachinery*, **113**, 331 (1991)